Mechanisms of Multidecadal Atlantic Meridional Overturning Circulation Variability Diagnosed in Depth versus Density Space

YOUNG-OH KWON

Woods Hole Oceanographic Institution, Woods Hole, Massachusetts

CLAUDE FRANKIGNOUL

Sorbonne (UPMC, University of Paris 06)-CNRS-IRD-MNHN, LOCEAN/IPSL, Paris, France

(Manuscript received 26 March 2014, in final form 15 September 2014)

ABSTRACT

Multidecadal variability of the Atlantic meridional overturning circulation (AMOC) is examined based on a comparison of the AMOC streamfunctions in depth and in density space, in a 700-yr present-day control integration of the fully coupled Community Climate System Model, version 3. The commonly used depth-coordinate AMOC primarily exhibits the variability associated with the deep equatorward transport that follows the changes in the Labrador Sea deep water formation. On the other hand, the density-based AMOC emphasizes the variability associated with the subpolar gyre circulation in the upper ocean leading to the changes in the Labrador Sea convection. Combining the two representations indicates that the ~20-yr periodicity of the AMOC variability in the first half of the simulation is primarily due to an ocean-only mode resulting from the coupling of the deep equatorward flow and the upper ocean gyre circulation near the Gulf Stream and North Atlantic Current. In addition, the density-based AMOC reveals a gradual change in the deep ocean associated with cooling and increased density, which is likely responsible for the transition of AMOC variability from strong ~20-yr oscillations to a weaker red noise–like multidecadal variability.

1. Introduction

The Atlantic meridional overturning circulation (AMOC) is a crucial component of the Atlantic as well as the global climate, for example through its close relationship with the meridional ocean heat transport (e.g., Msadek et al. 2013) and the Atlantic multidecadal oscillation (AMO; e.g., Knight et al. 2005). Although the AMOC is in nature a three-dimensional circulation, it is commonly studied in two-dimensional space, using the meridional overturning streamfunction, which is derived from the zonally integrated meridional velocity field. The most common representation of the AMOC streamfunction is in depth–latitude space, but an alternative representation is in density–latitude space. The two emphasize distinct aspects of the ocean circulation due to the difference in the zonal integration along a constant depth level versus along a constant density surface (Döös and Webb 1994; Mauritzen and Häkkinen 1999; Zhang 2010a). For example, the surface water gradually becomes denser as it travels with the cyclonic circulation of the North Atlantic subpolar gyre, but it stays at the same depth until it reaches convection sites. Therefore, AMOC in depth space tends to emphasize sinking (i.e., vertical mass flux) or isopycnal depth changes with latitude, while the AMOC in density space better represents the transformation of water mass property as a function of latitude (Straneo 2006; Pickart and Spall 2007).

Because deep observations are very limited in time and/or space, the AMOC and its long-term variability have been mostly investigated in climate model simulations. Many climate models exhibit a strong AMOC and AMO variability with a dominant time scale ranging from decadal to centennial, depending on the model. Simulations with the same climate model but with different ocean resolutions often show different dominant time scales (e.g., Bryan et al. 2006). Furthermore, some climate models exhibit more than one dominant AMOC time scales, or time-scale changes within a long integration

Corresponding author address: Dr. Young-Oh Kwon, Physical Oceanography Department, Woods Hole Oceanographic Institution, MS #21, Woods Hole, MA 02543.
E-mail: yokwon@whoi.edu

DOI: 10.1175/JCLI-D-14-00228.1

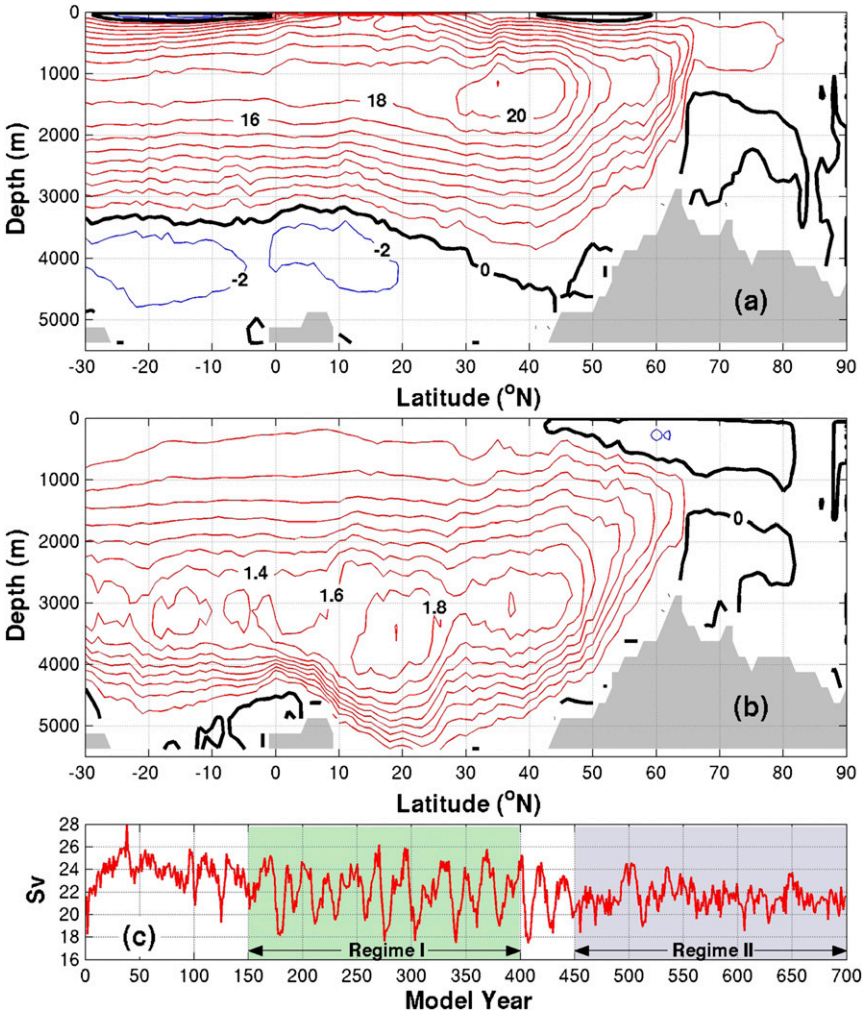

FIG. 1. (a) Mean AMOC streamfunction from the CCSM3 T85 control integration for the regime 1 (years 150–399). Positive values (red contours) indicate clockwise. The contour interval is 2 Sv. (b) Difference between the mean AMOC streamfunction of the two regimes [i.e., regime 1 (years 150–399) minus regime 2 (years 450–699)]. The contour interval is 0.2 Sv. (c) Time series of maximum annual mean AMOC strength at 35°N.

(Delworth and Greatbatch 2000; Hawkins and Sutton 2007; Danabasoglu 2008; Zhu and Jungclaus 2008). Therefore, it is important to understand the mechanisms that control the multidecadal AMOC variability and its possible changes in regime.

The 700-yr-long present-day control integration of the Community Climate System Model, version 3 (CCSM3; Collins et al. 2006), exhibits two very distinct regimes of the multidecadal AMOC variability (Danabasoglu 2008; Kwon and Frankignoul 2012). For about 250–300 years starting around the model year 150, CCSM3 shows a strong AMOC variability with ~20-yr periodicity (hereafter regime 1 or the strong oscillatory regime; Fig. 1c). Around model year 450, the AMOC regime suddenly changes to a more irregular and weaker red noise–like variability without a strong spectral peak (hereafter regime 2 or the red noise–like regime; Fig. 1c).

Focusing on regime 1, Danabasoglu (2008) found that the North Atlantic Oscillation (NAO) plays a prominent role in driving the AMOC variability, with a maximum correlation when a positive NAO leads an AMOC intensification by approximately 5 yr. As the NAO also exhibits a significant ~20-yr spectral peak, he discussed the possibility of a two-way ocean–atmosphere coupled mode associated with the strong oscillatory behavior of AMOC in regime 1. However, he concluded the evidence is not conclusive. On the other hand, Tulloch and Marshall (2012) suggested from their analysis of the same CCSM3 simulation that the strong ~20-yr AMOC variability is primarily associated with the upper ocean density changes

near the tail of the Grand Banks in the western North Atlantic and their advection around the subpolar gyre, hence essentially reflecting an ocean-only mode with atmospheric variability only acting as stochastic forcing.

In the red noise–like regime 2, Kwon and Frankignoul (2012) found the enhanced deep water formation in the Labrador Sea in response to the positive NAO is followed by the northward shift of the Gulf Stream–North Atlantic Current and a slightly contracted subpolar gyre near the eastern boundary. Resulting anomalous horizontal advection and vertical mixing over the shelf break along the eastern boundary generate denser anomalies in the upper ocean, which are subsequently transported into the Labrador Sea convection site, thereby sustaining the persistence of the deep water formation and the resulting AMOC intensification. They concluded that the red noise–like AMOC variability is primarily an ocean-only mode stochastically forced by the NAO surface fluxes, a similar conclusion to Tulloch and Marshall's (2012) for regime 1.

Frankignoul et al. (2013) examined the AMOC-to-atmosphere feedback and found in regime 2 that weak but significant atmospheric circulation anomalies resembling a positive NAO were following the stronger AMOC. As the AMOC intensification is driven by the positive NAO in the first place, this implies a weak positive feedback between the AMOC and the NAO, which would enhance the low-frequency power of the ocean-only mode suggested by Kwon and Frankignoul (2012). In regime 1, Frankignoul et al. (2013) found no direct evidence of AMOC influence on the atmosphere. However, upper ocean heat content anomalies resembling the AMOC footprint were found to precede the negative NAO, albeit lacking robustness, which hints at a weak negative feedback that should contribute to the oscillatory character of regime 1. In any case, there was no strong evidence supporting the existence of an ocean–atmosphere coupled mode.

Based on the above findings, both the strong AMOC oscillation in the regime 1 and the weak red noise–like AMOC variability in the regime 2 are likely ocean-only modes associated with the subpolar gyre advection. However, several questions remain to be answered: What determines the ~20-yr time scale in regime 1? What is the key difference between the two regimes that lead to such a different AMOC behavior? What led to a sudden transition between them? Furthermore, all of the above studies found that large anomalies along the Gulf Stream and North Atlantic Current are closely related to the AMOC variability, a northward shift of the ocean currents following a stronger AMOC. Why does the Gulf Stream and North Atlantic Current shift northward after the AMOC has intensified in CCSM3 (as in many other models), while observations and a few other models suggest the opposite shift (Kwon et al. 2010)? In this paper, we address these outstanding questions, primarily using the complementary information from the two distinct representations of AMOC streamfunction (i.e., in depth and in density spaces). In section 2, the model and analysis methods are briefly described. The mean AMOC streamfunctions in density and depth spaces are compared in section 3, and the 20-yr time scale selection of the AMOC oscillation in regime 1 is discussed in section 4. In section 5, the key differences and the transition between the two regimes are discussed. Conclusions are presented in section 6.

2. Model description and analysis methods

The 700-yr present-day control integration (i.e., the greenhouse gas concentrations fixed at the 1990 level) of CCSM3 at T85 × 1 is described by Collins et al. (2006). The Community Atmosphere Model, version 3 (CAM3), with 26 vertical levels and spectral T85 horizontal resolution (~1.4° resolution) is the atmospheric component. The ocean component is the Parallel Ocean Program version 1.4 (POP1.4), which has a zonal resolution of 1.125° and a meridional resolution of 0.27° at the equator gradually increasing to a maximum of approximately 0.6° at about 40°N. Vertically, there are 40 levels, whose thickness monotonically increases from 10 m near the surface to 250 m in the deep ocean below 1500 m. The land and sea ice components are the Community Land Model version 3 (CLM3), and the Community Sea Ice Model version 5 (CSIM5), which have the same horizontal resolution as the atmosphere and ocean component models, respectively.

The AMOC streamfunctions are calculated based on the monthly mean fields to take into account the seasonal correlation between the density and velocity, which especially affects the AMOC in density space. Potential density referenced to the 2000-dbar level (σ_2) is used for the density space AMOC, and the density axis is chosen to be proportional to the mean volume of the each density layer in the Atlantic to the north of 30°S (Fig. 2a), to facilitate the comparison with the AMOC in depth space. All the analyses are based on annual means. The empirical orthogonal functions (EOFs) are computed from the covariance matrix of input time series, and are displayed as regression maps on the corresponding normalized principal component (PC), so that the EOFs show the typical amplitude of the fluctuations. All time series are linearly detrended in each analysis period, unless noted otherwise. The statistical significance of the correlation or regression coefficients is assessed with a two-sided Student's t test using an

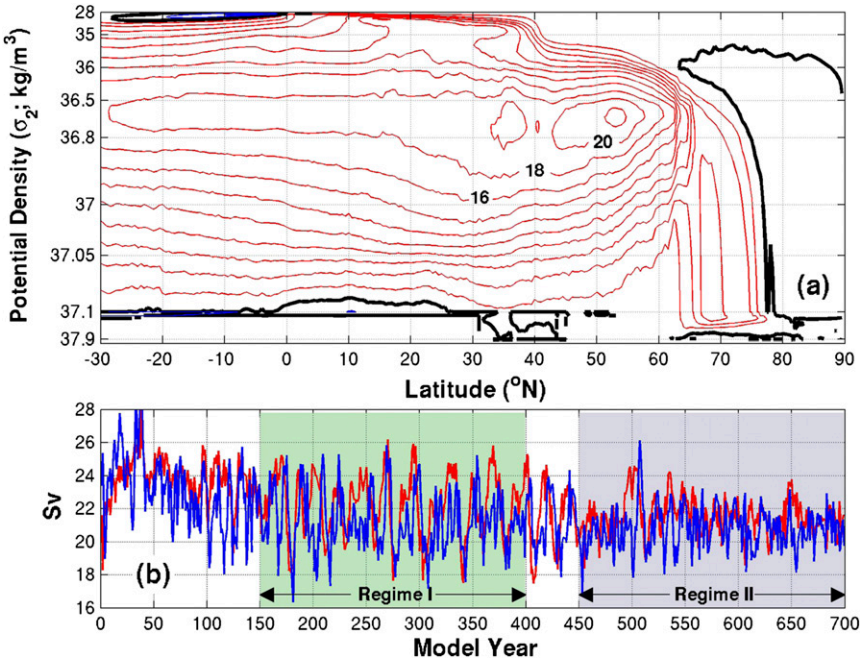

FIG. 2. (a) Mean AMOC streamfunction on density coordinate (σ_2) in regime 1. Note that the vertical coordinate is stretched to be proportional to the volume of each density layer. Positive values (red contours) indicate clockwise. The contour interval is 2 Sv. (b) Time series of maximum annual mean AMOC strength at 56°N from the AMOC on density coordinate (blue curve), and at 35°N from the AMOC on depth coordinate (red curve: as in Fig. 1c).

effective temporal degree of freedom taking into account the serial autocorrelation at lag 1 (Trenberth 1984; Bretherton et al. 1999).

3. Mean AMOC streamfunctions in depth and density spaces

The basic features of the North Atlantic ocean circulation in CCSM3 have been presented in Danabasoglu (2008), Kwon and Frankignoul (2012), Tulloch and Marshall (2012), and Frankignoul et al. (2013). Here we briefly discuss the mean fields in regime 1. The mean fields in regime 2 are very similar, with an approximately 10% weaker amplitude and slight spatial displacements, as illustrated in Figs. 1b and 3b,d. These differences will be discussed in section 5.

The upper 500-m mean circulation (Fig. 3a) shows that the Gulf Stream, the North Atlantic Current, and the subpolar gyre are somewhat broader and weaker than in observations. In addition, the northern recirculation gyre and the northwest corner are not present, which is typical of global climate models with limited horizontal resolution in the ocean. Furthermore, the Nordic seas overflow is poorly simulated, unlike in more recent versions with a new overflow parameterization (Danabasoglu et al. 2012). The primary deep water formation site in this model (marked by the green box in Fig. 3) is found in the western subpolar gyre; weaker convection occurs in the Irminger Sea and Nordic seas (Kwon and Frankignoul 2012). The interannual and longer variability of the winter mixed layer depth is also concentrated near the main convection site.

The deep circulation (2000–3000 m) exhibits the cyclonic boundary current in the subpolar gyre, but there is no well-defined Deep Western Boundary Current between the Flemish Cap and Cape Hatteras (Fig. 3c). Instead, the deep equatorward flow detaches from the western boundary near the Flemish Cap and follows an interior path along the western flank of the Mid-Atlantic Ridge. It then returns to the western boundary near Cape Hatteras. It is noteworthy that the interior pathway is similar to that suggested by recent observation and an eddy-resolving ocean model (Bower et al. 2009).

In depth space, the mean AMOC exhibits a maximum strength of almost 22 Sv (1 Sv $\equiv 10^6\,\mathrm{m^3\,s^{-1}}$) near 35°N and 1200 m, with the standard deviation of approximately 4 Sv in regime 1 (Fig. 1). There are two rather distinct sinking branches near 62° and 47°N, respectively. The former is associated with deep convection in the subpolar gyre and the sinking of Nordic seas overflow water, whereas the latter is due to the abrupt

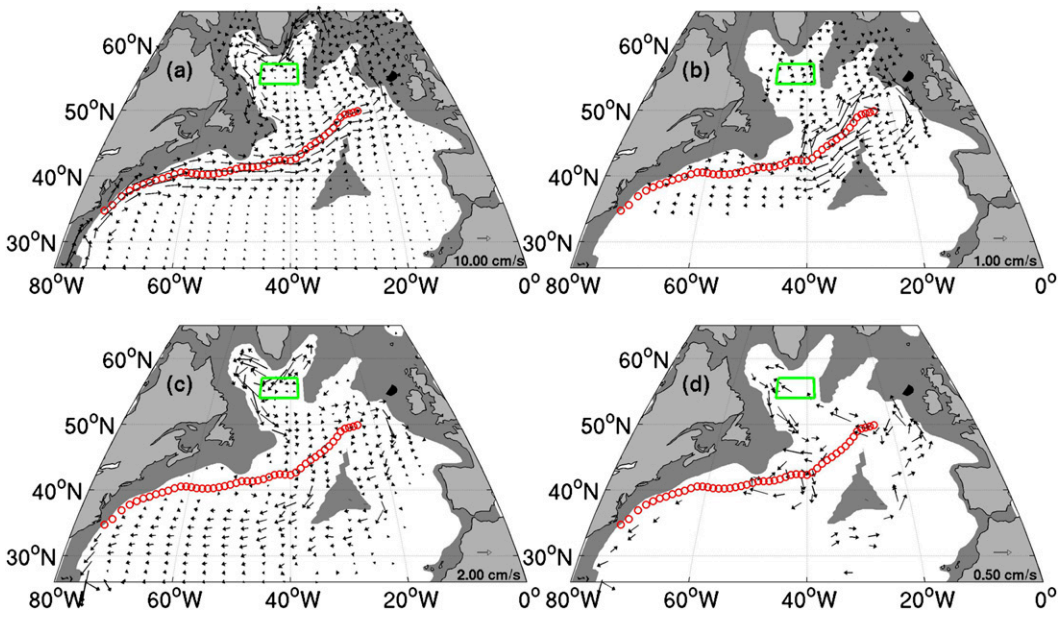

FIG. 3. (a) Mean upper ocean velocity (0–500-m average) in regime 1. (b) Difference in the mean upper ocean velocity between the two regimes (i.e., regime 1 minus regime 2). (c),(d) As in (a),(b), but for the deep ocean velocity (2000–3000-m average). Red circles indicate the mean position of the Gulf Stream–North Atlantic Current defined as location of the maximum upper 500-m velocity. Green boxes denote the main convection site in this simulation. The region shallower than 2500 m is indicated with the gray shading.

deepening of isopycnal surfaces when the equatorward flow coming from the subpolar gyre slides underneath the northward flowing Gulf Stream and North Atlantic Current, as discussed in section 4. The meridional velocity in a zonal section along 40°N (Fig. 4b), close to the AMOC maximum, clearly shows that the northward flow is concentrated in the Gulf Stream in the upper ocean and the equatorward return flow is found at depth. Therefore, the maximum meridional overturning at this latitude is primarily achieved by the crossover between the northward flow in the upper ocean and the deep equatorward flow. Note that the isopycnal surfaces are overall level at this latitude, implying that the AMOC calculated in depth and density spaces should be similar.

In density space, the mean AMOC is a maximum near 54°N (Fig. 2a). Its downward branch, concentrated near 62°N, is associated with dense water formation. There is a secondary AMOC maximum near 35°N, at the same location and with similar amplitude as the maximum in the depth AMOC, due to the level isopycnal surfaces, as already pointed out. North of about 40°N, its upper branch becomes gradually denser toward the north, as heat from the warm surface water is gradually lost to the cold atmosphere (thus densifying the upper ocean) while the surface water is advected along North Atlantic Current and the subpolar gyre. The water mass transformation in the Nordic seas (north of 65°N) is also more clearly represented than in depth space. The meridional velocity along 56°N (Fig. 4a) reveals a very different situation in the subpolar domain from that at 40°N and in the subtropics. Indeed, the isopycnal surfaces are not flat, but strongly doming near the main convection site. Therefore, zonal integration along a constant depth and a constant density surface results in very different AMOC amplitudes. In addition, the northward flow at 56°N is largely found in the eastern half of the subpolar gyre while the equatorward flow is in the western half. As the equatorward flow is relatively more barotropic than the northward flow due to gradual buoyancy loss and densification along the cyclonic subpolar gyre (Straneo 2006), the meridional overturning at this latitude is a result of the east–west contrast between the baroclinic northward flow and more barotropic equatorward flow, unlike the upper and deep ocean contrast in the subtropics. Difference in the water depth between the eastern and western basins also contributes to the east–west contrast in the current structures.

4. The AMOC variability in regime 1

a. Comparison between the AMOC variability in depth and density spaces

The variability of AMOC at the latitude of its respective maximum in depth and density spaces is highly correlated and has very comparable amplitudes, in particular

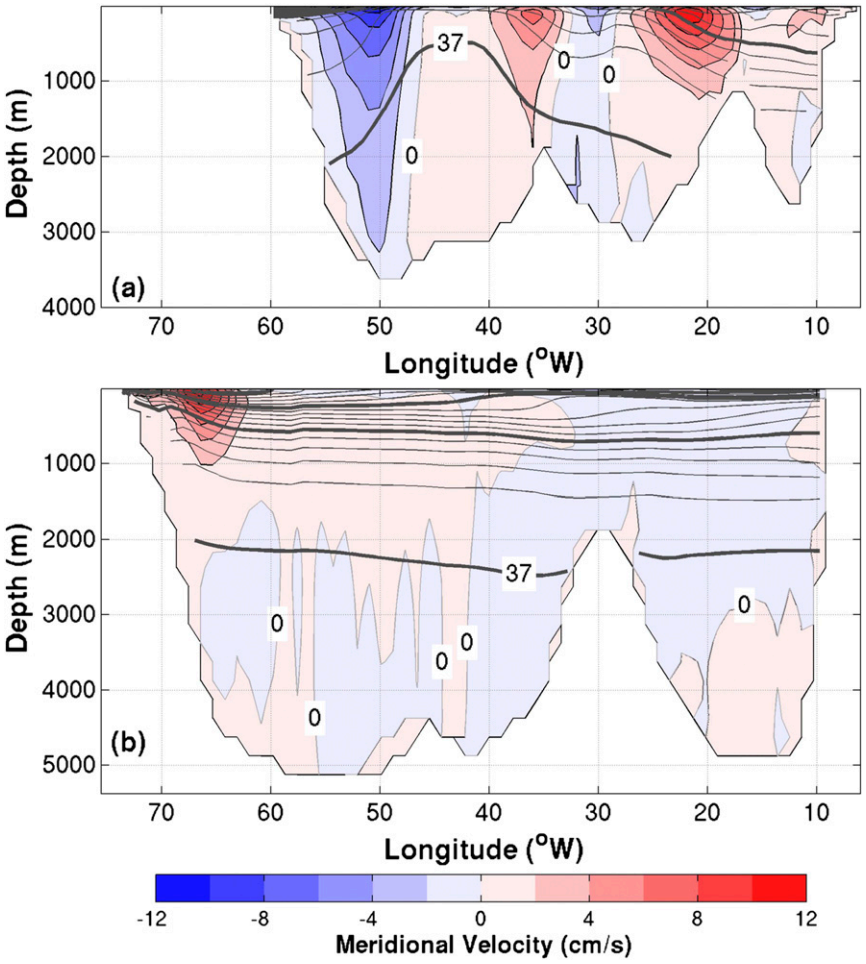

FIG. 4. Mean meridional velocity (shadings) and density (σ_2; black contours) along a zonal section at (a) 56°N and (b) 40°N in regime 1. Contour intervals are 2 cm s^{-1} and 0.2 kg m^{-3}, respectively.

for the regime 1 (Fig. 2b). The maximum correlation (r = 0.52) is found when the depth AMOC time series at 35°N leads the density AMOC time series at 56°N by 3 yr. This relationship does not change when the latitude of the maximum AMOC amplitude is allowed to vary at each time step. The phase relationship is seemingly contradictory to our general notion that the AMOC variability is primarily driven by the deep water formation changes in high latitude, and thus propagates from north to south (e.g., Zhang 2010b; Kwon and Frankignoul 2012). In depth space, the lag correlation between anomalous AMOC amplitude at each latitude and a reference latitude taken at 35°N indeed exhibits a propagation of AMOC anomalies from north to south as expected (Fig. 5a). However, the density space provides a different picture, as the AMOC anomalies propagate northward north of 40°N (in the subpolar region) and southward to the south (Fig. 5b). Note that the results are not sensitive to the choice of reference latitude. This striking difference will lead below to a better understanding of the 20-yr time scale in regime 1.

b. *Meridional propagation of AMOC anomalies in depth space*

Changes in the equatorward propagation speed as a function of latitude are apparent in the lag correlation of AMOC anomalies in depth space (Fig. 5a). The anomalies are almost simultaneous in 50°–60°N, and then the propagation takes them approximately 2 yr from 50° to 40°N. Finally, the propagation speeds up again to the south of 40°N, so that they reach the equator in little more than a year. These AMOC anomalies are primarily associated with the deep density anomalies following the deep water formation variability.

This is best seen by considering the evolution of three-dimensional patterns of the AMOC anomalies at depth.

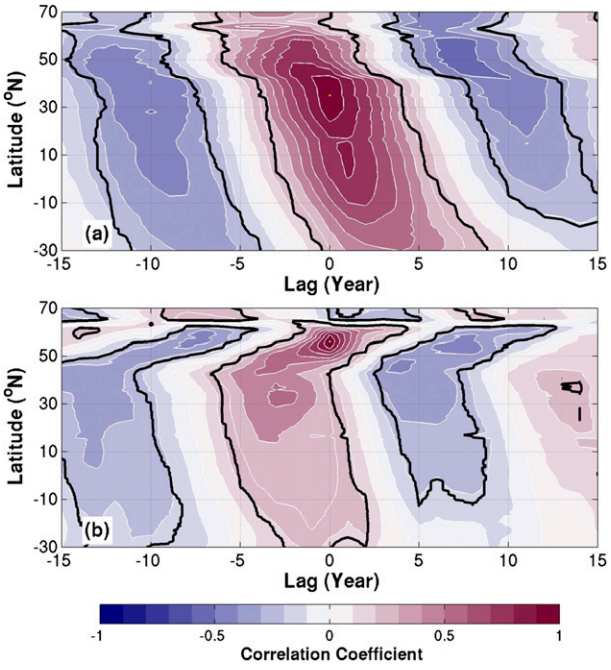

FIG. 5. Lag correlation between the maximum AMOC time series at each latitude and the one at a fixed base latitude in regime 1 from (a) depth coordinate AMOC using 35°N as the base latitude and (b) density coordinate AMOC using 56°N as the base latitude. Contour interval is 0.1. Black contours indicate the significance at the 5% level.

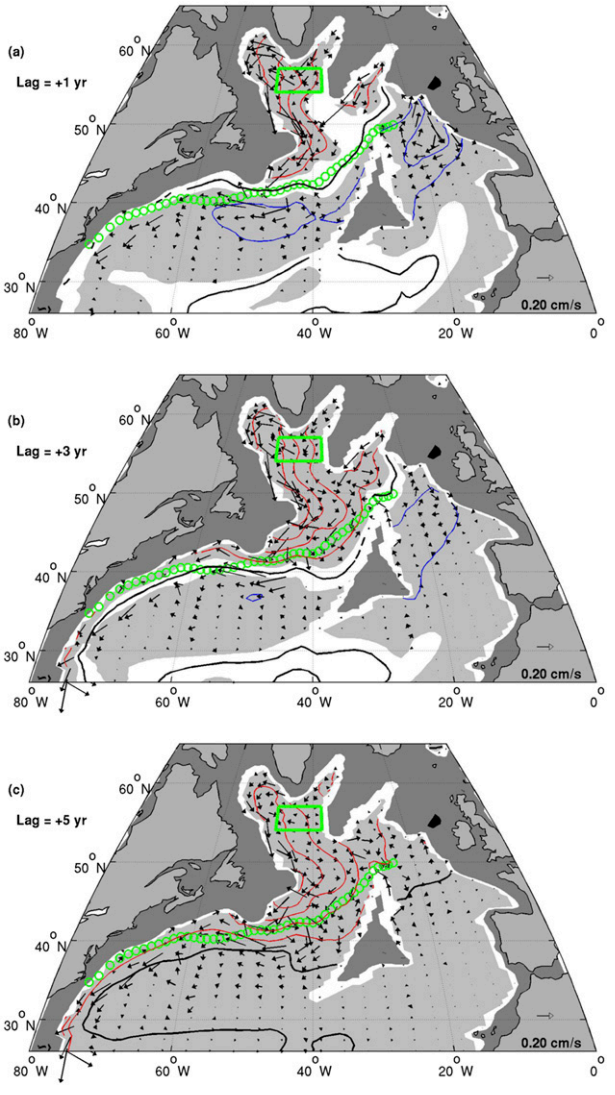

FIG. 6. Lag regression of 2000–3000-m density (σ_2; 0.002 kg m^{-3} contour interval) and velocity (arrows) on the convection index in regime 1. Positive (negative) density anomalies are plotted in red (blue). Light shading indicates significance at the 5% level for the density regression. Lag is positive when the convection index time series leads. The green boxes denote the location of the convection site. Green circles indicate the mean position of the Gulf Stream–North Atlantic Current defined as location of the maximum upper 500-m velocity.

Figure 6 shows the lag regression of the 2000–3000-m circulation and density anomalies onto the time series of convection that was shown by Kwon and Frankignoul (2012) to play a key role in driving the AMOC variations. The convection index is defined as the upper 500-m density averaged over the main convection site (54°–57°N, 38°–48°W; green box in Fig. 3). The denser anomalies formed near the convection site take about 1–2 yr to reach the western boundary and sink (Fig. 6a), as described in more detail by Kwon and Frankignoul (2012). As the denser anomalies are concentrated near the subpolar western boundary at lag = 1 yr, the corresponding anomalous equatorward geostrophic current is also concentrated near the same region (Fig. 6a). Two years later (lag = 3 yr), the deep denser anomalies have propagated farther equatorward, even reaching the southern limit of the domain, along the very narrow western boundary topographic waveguide, presumably as a topographic Rossby wave. At the same time, the anomalous equatorward velocity expands into the interior near 40°–50°N as the denser anomalies are advected along the slower interior pathway toward the western flank of the Mid-Atlantic Ridge (Fig. 6b). Finally at lag = 5 yr when the AMOC regression on the convection index is maximum (Fig. 7e), the deep density and corresponding velocity anomalies along the interior path and western boundary become well connected (Fig. 6c). Therefore, the meridional propagation of the AMOC anomalies in depth space primarily reflects the changes in the deep equatorward branch of the AMOC. A similar scenario, albeit based on density AMOC, was suggested by Zhang (2010b).

The unidirectional equatorward propagation of the AMOC anomalies in depth space can be also seen in the

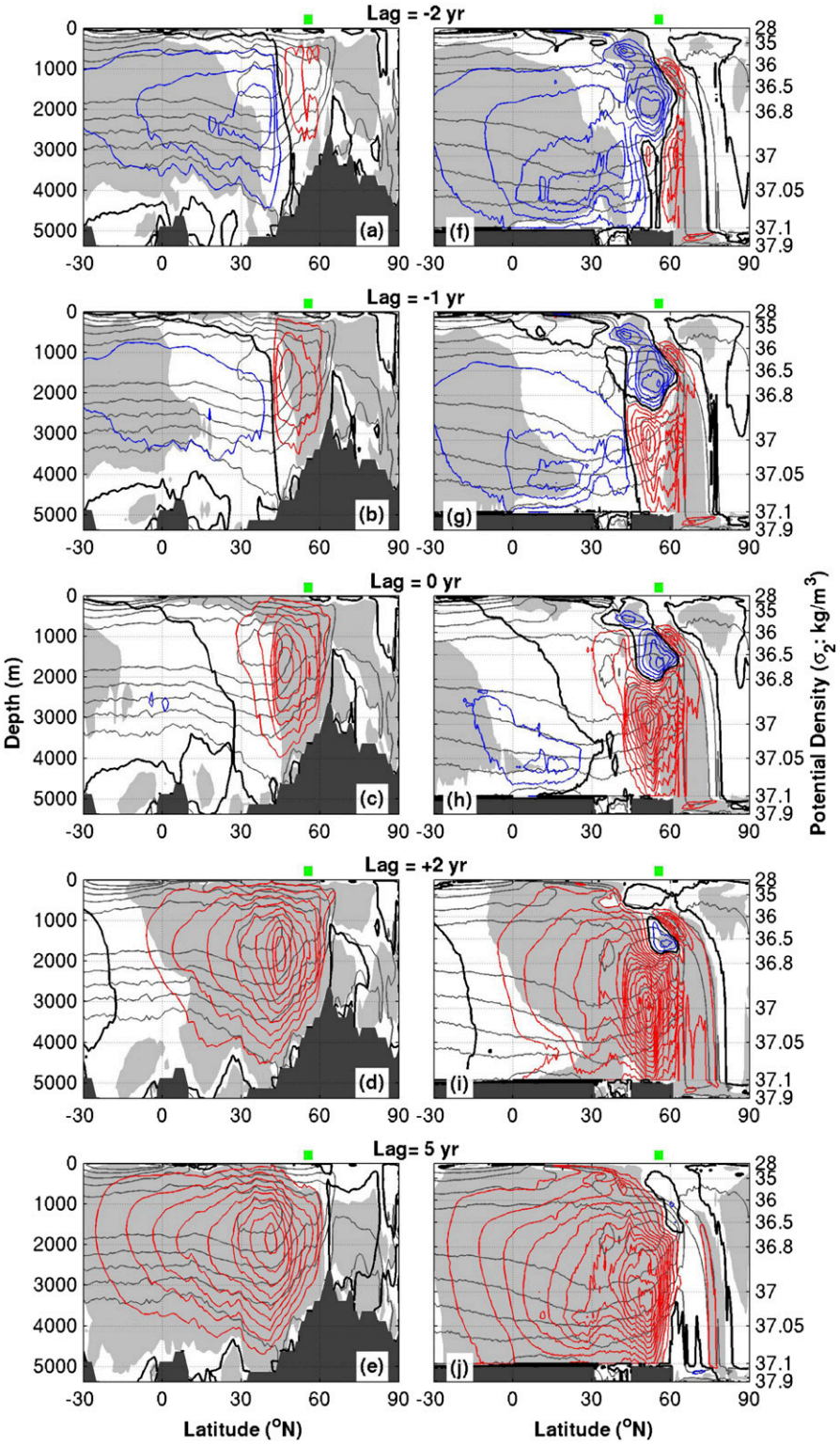

FIG. 7. Lag regression of the AMOC on the convection index in regime 1 based on (a)–(e) depth coordinate AMOC and (f)–(j) density coordinate AMOC. Contour interval is 0.2 Sv, and the positive (negative) values are plotted in red (blue). Shading indicates significance at the 5% level. Positive lags indicate AMOC lagging the convection index time series. The green bars denote the location of the convection site. The mean AMOC is plotted in gray contours in 4-Sv intervals.

lag regressions on the convection index (Figs. 7a–e, where the mean AMOC streamfunction is overlaid as gray contours). Two years prior to the maximum convection, the AMOC begins to strengthen in the subpolar region (Fig. 7a). Note that the negative anomalies (i.e., the blue contours) are associated with the preceding minimum convection event but appear here because of the strong ~20-yr oscillation. Subsequently, the AMOC gradually strengthens and expands equatorward, as shown by many previous studies (e.g., Deshayes and Frankignoul 2008), reaching their maximum 5 yr after the maximum convection (Fig. 7e). Hence, in depth space, the anomalies propagate similarly southward in the upper and lower branches of the AMOC. This apparent simplicity hides a complex behavior best understood in density space.

c. *Meridional propagation of AMOC anomalies in density space*

Two years prior to the maximum deep convection, the AMOC also begins to strengthen in density space, but in a narrower latitude band near 60°N, while farther south the AMOC is weaker than normal, reflecting the previous weakening phase (Figs. 7f–j). For example, the opposite signed counterpart to the strong negative anomalies around $\sigma_2 = 36.7$ and 55°N appears at lags 8–10 yr. Subsequently, the density AMOC also strengthens and expands equatorward, but initially only in the deeper/denser branch (Figs. 7g,h). Around lag 0, when the density AMOC anomalies reached the boundary between the subpolar and subtropical gyres (40°–50°N), the anomalies begin to propagate upward toward the upper/lighter branch (Fig. 7h). Then, the density AMOC anomalies further expand equatorward in the full water column south of the gyre boundary and, at the same time, propagate northward in the upper/lighter branch in the subpolar region, reaching their full extent in about 2 yr (Figs. 7i,j). Therefore, the peculiar meridional propagation of the AMOC anomalies in Fig. 5b seems to be due to the different propagations in the upper and deeper branch of the density AMOC.

This is clearly seen by separately considering the meridional propagations of the density AMOC anomalies in the upper and deeper branches, based on the lag correlation between the AMOC anomalies at each latitude and the convection index (Fig. 8). Indeed, the deeper branch exhibits the unidirectional equatorward density AMOC propagation (Fig. 8b), very similar to the depth AMOC propagation (Fig. 5a). Note that the equatorward propagation of the maximum AMOC anomalies begins at approximately 60°N about one year after the maximum convection and reaches the gyre boundary (~40°N) at lag = 5 yr, which is consistent with the 2000–3000-m circulation and density anomalies shown in Fig. 6.

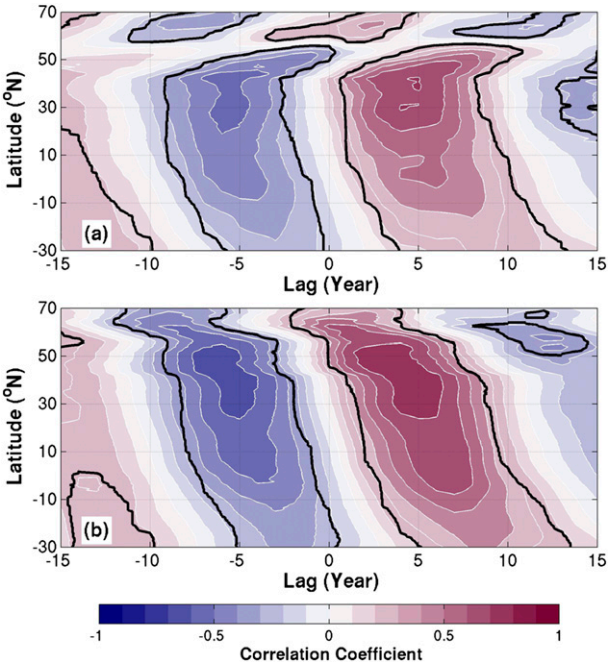

FIG. 8. Lag correlation between the convection index and the AMOC time series at each latitude averaged over (a) $35.5 < \sigma_2 < 36.5$ and (b) $36.8 < \sigma_2 < 37.1$ in regime 1. Contour interval is 0.1. Black contours indicate the significance at the 5%.

On the other hand, the density AMOC anomalies in the upper branch propagate northward to the north of 40°N (Fig. 8a). The northward propagation in the upper ocean is associated with the advection of the density anomalies along the cyclonic subpolar gyre as shown in Fig. 9. Note that we will focus on the northward propagation of negative AMOC anomalies prior to the maximum convection (i.e., the blue anomalies in Fig. 8a), which allows us to explain better the continuous chain of events linking the upper ocean anomalies before the maximum convection and the deep anomaly propagations after the convection. Nine years prior to the maximum convection, the positive upper 500-m density anomalies appear along the mean path of the North Atlantic Current near the western flank of the Mid-Atlantic Ridge (MAR) (Fig. 9a), indicating the southward shift of the North Atlantic Current path [as the Gulf Stream (GS)–North Atlantic Current (NAC) is a strong density front, a shift in a cross-frontal direction results in density anomalies centered around its mean path]. In subsequent years, the positive density anomalies become stronger until 5 yr prior to maximum convection, and then circulate cyclonically around the subpolar gyre, eventually filling the entire subpolar gyre, including the main convection site at lag = 0 (Figs. 9b,c).

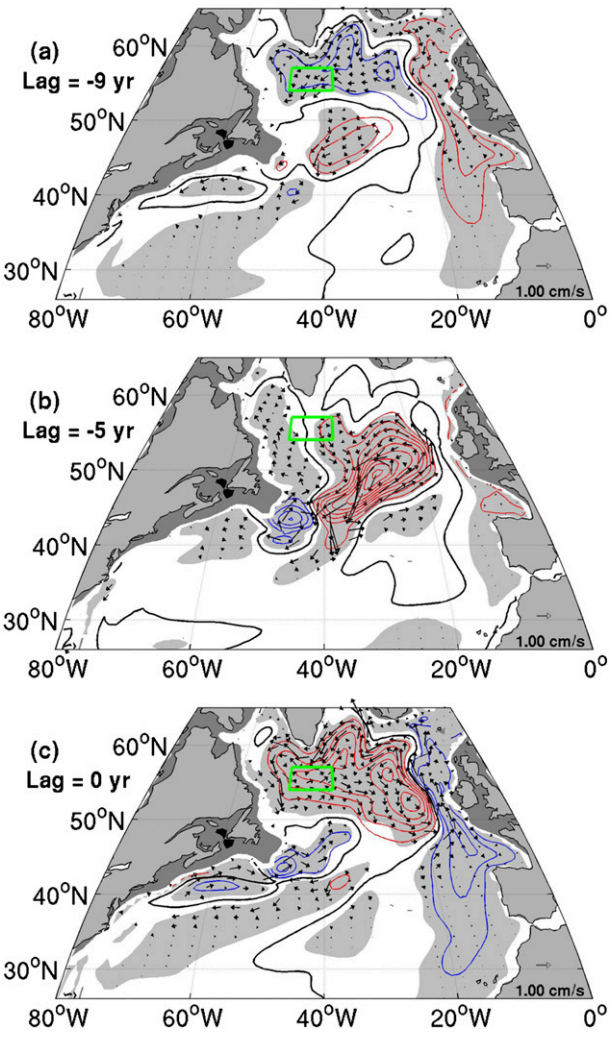

FIG. 9. Lag regression of upper 500-m density (σ_θ; 0.02 kg m^{-3} contour interval) and velocity on the convection index in regime 1. Positive (negative) density anomalies are plotted in red (blue). Light shading indicates significance at the 5% level for the density regression. Lag is positive when the convection index time series leads. The green boxes denote the location of the convection site.

While the northward direction of positive density anomaly advection coincides with the northward propagation of the density AMOC anomalies in the upper ocean, two questions remain: 1) Why does the propagation of a positive density anomaly correspond to that of the negative density AMOC anomaly? 2) Why does the North Atlantic Current path shift southward to create the positive density anomalies in the first place, and why do they strengthen with time? To address the first question, recall that the sloping surface branch in the density AMOC to the north of 40°N (Fig. 2a) reflects the gradual heat loss from the warm surface water to the atmosphere as it is advected northward along the subpolar gyre. Hence, the upper layer density is lighter in the eastern part of subpolar gyre, and there is even no corresponding density class in the western part (Fig. 4a). The surface branch of the density AMOC is thus dominated by the eastern subpolar gyre, where the positive density anomalies in the upper ocean propagate northward while intensifying. This results in a shift of AMOC surface branch toward slightly denser values with increasing latitude and the northward propagation of negative upper AMOC anomalies on fixed density surfaces.

To answer the second question, one has to consider the crossover of the shallow and the deep AMOC branches, and their interaction with topography. The southward shift of the North Atlantic Current path in several years prior to the maximum convection (Fig. 9) is associated with the weaker deep equatorward flow (and weaker AMOC) resulting from the previous minimum convection event as a part of the ~20-yr cycle. Previous studies have suggested that the Gulf Stream path shifts southward in response to the stronger deep current based on theoretical models (Thompson and Schmitz 1989; Spall 1996a,b), observations (Peña-Molino and Joyce 2008), and general circulation models (Zhang and Vallis 2007), which is seemingly opposite to what occurs in CCSM3. However, most of these studies focused on the role of bottom topography along the western boundary. When the equatorward Deep Western Boundary Current (DWBC) encounters the Gulf Stream near the Cape Hatteras, it moves downslope and offshore to about 1000 m deeper bottom depth to conserve the potential vorticity (Hogg and Stommel 1985; Figs. 10a–c). In addition, the bottom Ekman transport moves the current farther downslope, so that the bottom vortex stretching induced by a downslope DWBC leads to an enhanced cyclonic northern recirculation gyre and a Gulf Stream located farther south (Zhang and Vallis 2007; Figs. 10a–c).

On the contrary, as described in section 3, the crossover between the surface Gulf Stream–North Atlantic Current and the deep return flow primarily occurs near the western flank of the Mid-Atlantic Ridge in CCSM3 (Figs. 3 and 11a). There are two important differences between the western boundary and the western flank of the Mid-Atlantic Ridge. First, the bottom slope is at least twice less steep on the western flank of the Mid-Atlantic Ridge. As on the western boundary, the deep equatorward flow moves downslope when it encounters the North Atlantic Current, as can be seen from the mean downwelling over the slope (Fig. 11b). However, with the gentler slope the flow cannot just move to deeper bottom depth, but the water column has to squeeze and generate anticyclonic vorticity, opposite to the western boundary case. The meridional velocity

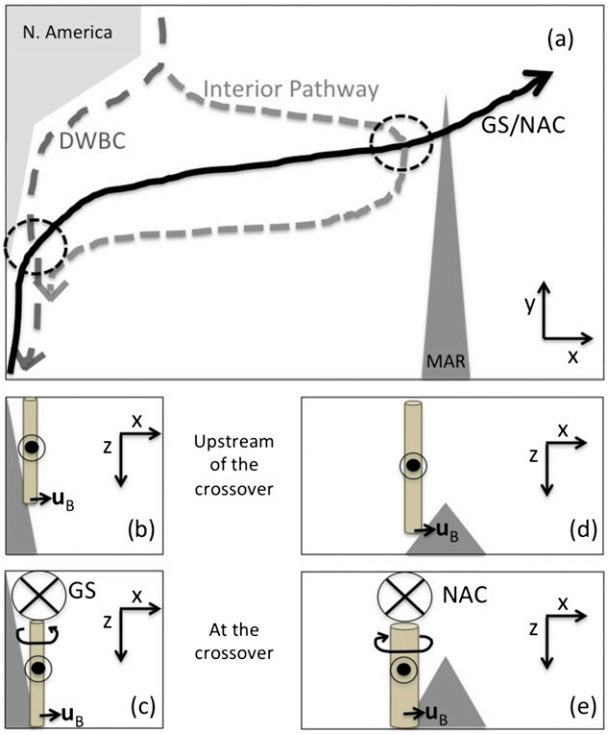

FIG. 10. Schematic diagram of the crossover between the deep equatorward return flow and the poleward GS–NAC in the upper ocean. (a) Plan view with the two different pathways for the deep equatorward return flow: the classical DWBC and the interior pathway, indicated with the dashed curves, and the GS–NAC with the solid curve. Two different crossover locations, on the western boundary and the western flank of the MAR, are indicated with the dashed circles. (b),(c) Side view from the south of the crossover on the western boundary. Upstream of the crossover in (b), the barotropic equatorward current flows along relatively shallower isobath (~3200 m; Hogg and Stommel 1985), until it dives ~1000 m downslope underneath the GS at the crossover in (c). The bottom Ekman transport ($\mathbf{u}_B$) pushes the DWBC farther downslope, causing vortex stretching. Therefore, an increased deep flow would result in anomalous cyclonic vorticity at the crossover and a southward shift of GS. (d),(e) Side view from south for the crossover on the western flank of MAR. Because of upstream deeper water depth and much gentler slope at the crossover, there is vortex compression when the equatorward deep flow passes underneath the NAC. In addition, the upslope bottom Ekman transport also causes vortex compression. Therefore, an increased deep flow would result in anomalous anticyclonic vorticity and northward shift of NAC.

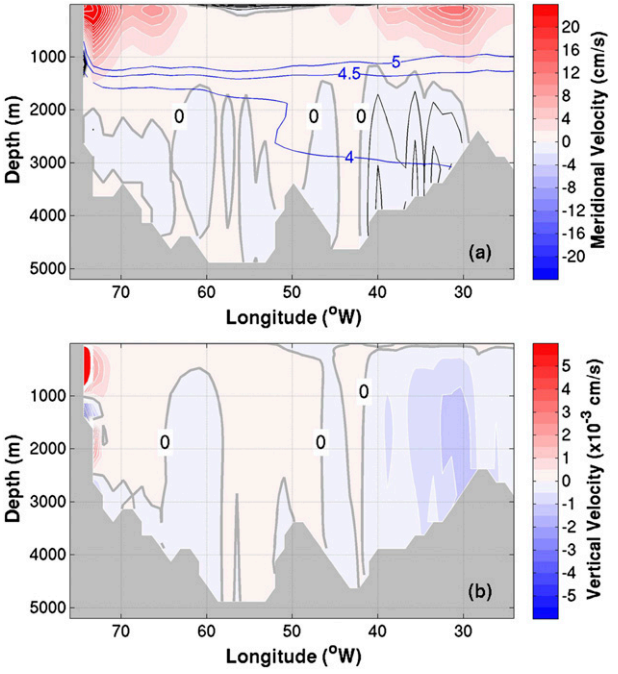

FIG. 11. Mean (a) meridional and (b) vertical velocity in regime 1 along the mean path of the GS–NAC (denoted with the red circles in Fig. 3). Contour intervals are 2 cm s^{-1} and 5 × 10^{-4} cm s^{-1}, respectively. Note the additional black contours for −0.5 and −1 cm s^{-1} in (a), as well as the blue contours for 4°, 4.5°, and 5°C potential temperature isotherms.

sections in Fig. 12 show that the deep return flow originating from the Labrador Sea separates in two branches of equatorward flow in the subpolar gyre, with the stronger equivalent barotropic branch at 48°N on the western boundary and a weaker deep branch along the western flank of the Mid-Atlantic Ridge. They merge south of 45°N as one deep equatorward flow along the western flank of the Mid-Atlantic Ridge, which goes underneath the North Atlantic Current (Fig. 11). The height of water column indicated by the 5°C isotherms changes from about 4000 m for the equivalent barotropic branch to about 3000 m for the deep flow at the crossover, illustrating the strong vortex squeezing (Figs. 11a and 12).

Another important difference is the opposite bottom slope. With the bottom depth decreasing eastward on the western flank of the Mid-Atlantic Ridge, the bottom Ekman transport associated with the equatorward deep flow is upslope, which opposes the downslope mean flow and also generates anticyclonic vorticity. These two factors cause the shift of the surface currents in response to the changes in the deep flow to be opposite at the two locations, while the dynamics are the same. Therefore, the southward shift of the North Atlantic Current path in response to the weaker deep return flow near the western flank of the Mid-Atlantic Ridge in CCSM3 is actually consistent with the studies focusing on the crossover near the western boundary. Furthermore, with the gradual weakening of the anomalous deep return flow on the western flank of the Mid-Atlantic Ridge between about year −10 and −5 (Fig. 8b, around 48°–50°N), the shift of the North Atlantic Current path and the upper ocean density anomalies correspondingly intensify until lag = −5 yr (Fig. 9).

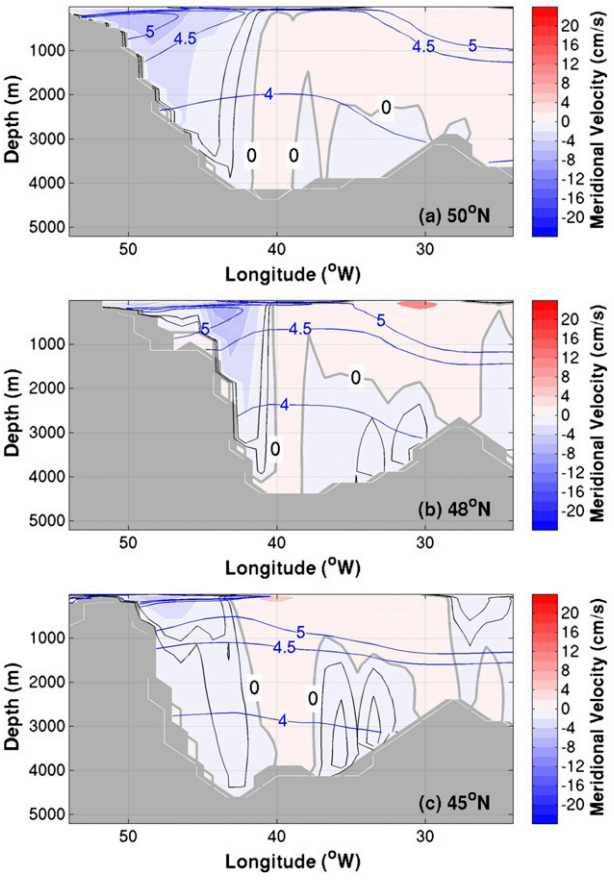

FIG. 12. As in Fig. 11a, but for the zonal section at (a) 50°, (b) 48°, and (c) 45°N.

d. The 20-yr time scale selection

With the above clarification, the northward propagation of the AMOC anomalies in density space to the north of 40°N can be explicitly attributed to the northward advection of density anomalies along the subpolar gyre in the upper ocean. We can now combine the information from the depth AMOC propagation mainly reflecting changes in the deeper branch following the maximum convection and that from the density AMOC propagation better showing the changes in the upper branch leading up to the maximum convection to explain the time scale selection of ~20-yr AMOC oscillation in the regime 1, as summarized with a schematic diagram in Fig. 13.

As we can start from anywhere in the diagram because of the strong oscillatory nature, we start from the bottom of the diagram (i.e., the minimum deep convection phase). The reduced deep convection results in decreased deep equatorward flow and weaker AMOC, which gradually propagates from north to south and reaches the gyre boundary (~40°N) approximately 5 years later. The weakened deep flow results in a southward shift of the surface North Atlantic Current path and positive density anomalies in the upper ocean near the western flank of the Mid-Atlantic Ridge. These positive density anomalies are subsequently advected northward and somewhat damped along the subpolar gyre, which corresponds to the northward propagation of the negative AMOC anomalies in the density space AMOC. After another 5 years, the whole subpolar gyre becomes denser and the convection reaches its maximum (top of the diagram). This half cycle from the minimum convection to the maximum convection takes approximately 10 yr with 5 yr for the deep equatorward anomaly propagation and the other 5 yr for the upper ocean northward advection within the subpolar gyre. Then the other half cycle with the opposite phase follows. Because the NAO directly affects deep convection, the feedback loop is both sustained and made irregular by stochastic NAO forcing.

5. Transition from regime 1 to regime 2

Around the year 450, the CCSM3 AMOC variability abruptly becomes weaker (i.e., the standard deviation decreases from approximately 4 Sv in regime 1 to approximately 2 Sv in regime 2) and irregular (Fig. 1c). The main difference between the mean AMOC in the two regimes is that the deep equatorward branch is slightly stronger and deeper in regime 1 (Fig. 1b), consistent with the stronger equatorward 2000–3000-m velocity along the western boundary of the subpolar/subtropical gyres and the interior path (Fig. 3d). In regime 1, the North Atlantic Current path is also slightly further north near the Mid-Atlantic Ridge (Fig. 3b) and the eastern half of the subpolar gyre slightly more contracted (Fig. 14a). Although these differences are small (only about 10% of the respective mean), they may be primarily responsible for the change from the ~20-yr time scale in regime 1 to the longer irregular time scale in the regime 2, as briefly pointed out by Kwon and Frankignoul (2012). Indeed, the slightly contracted and stronger eastern subpolar gyre in regime 1 carries the density anomalies originating from the meridional shift of the North Atlantic Current path to the convection site before they are damped by the surface heat flux, thus reversing the phase of the AMOC oscillation (Fig. 14b). The heat flux damping is 20–25 $W m^{-2} °C^{-1}$ along the North Atlantic Current path in CCSM3 (Frankignoul et al. 2013), so that approximately 10 yr are needed to damp temperature (or equivalently density) anomalies in a mixed layer of about 200-m depth. On the other hand, the slightly wider and weaker eastern subpolar gyre in regime 2 fails to advect the negative density

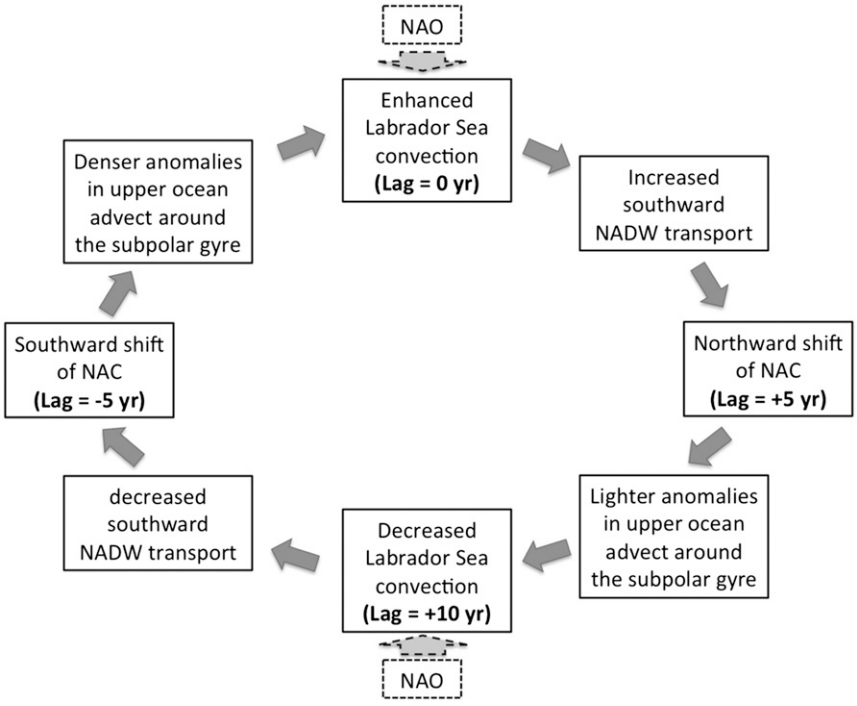

FIG. 13. Schematic diagram for the mechanism of 20-yr AMOC variability in regime 1 (NADW stands for North Atlantic Deep Water). Note that the dashed boxes and arrows indicate that the NAO acts as stochastic forcing, but does not determine the 20-yr time scale.

anomalies all the way to the convection site, which does not favor an oscillatory AMOC behavior (Fig. 14c; Kwon and Frankignoul 2012). Kwon and Frankignoul (2012) pointed out that the positive density anomalies that had developed along the eastern boundary (Fig. 14c) were slowly advected into the convection region and contributed to the long persistence of the convection and AMOC anomalies in regime 2. On the other hand, these positive density anomalies never get a chance to reach the convection site in regime 1, as the negative density anomalies along the North Atlantic Current block their way to the convection site (Fig. 14b) and initiate the opposite phase of the 20-yr oscillation.

Then what causes the sudden transition from the regime 1 to regime 2? To examine the transition, the EOFs of the AMOC in density space are calculated for the whole record length encompassing the two regimes, without detrending (Fig. 15). The leading EOF (explaining 47.3% of the total variance) is primarily associated with the multidecadal variability, while the second EOF (16.6% of the total variance) turns out to be related to a secular change. The second PC (PC2) reveals a gradual transition around the year 450 toward a stronger deep limb in the densest portion (below $\sigma_2 =$ 37.05) and a weaker deep limb in the lighter portion ($\sigma_2 = 36.50$–37.00) in regime 2 (Fig. 15b vs Fig. 2a). This change is associated with the deep subpolar ocean (2000–3000 m) becoming denser (Fig. 16a; note that the density axis is reversed), and it is well correlated with the gradual overall southward shift of the North Atlantic Current path shown with the 200-yr moving averaged time series in Fig. 16b.

The slowly increasing density in the deep subpolar ocean is likely a regional realization of the small drift in the CCSM3 global mean temperature toward colder temperature, especially below 1000 m (Collins et al. 2006), which is an unfortunate but typical climate model artifact. The resulting increase in the vertical stability in the subpolar gyre likely causes the slight shallowing (accompanied by the southward shift) of the winter mixed layer depth at the main deep convection site (Kwon and Frankignoul 2012), which leads to a more irregular and weaker AMOC and a southerly North Atlantic Current path. We tentatively speculate that the transition between the two regimes is not smooth because at some point the stochastic forcing may be strong enough to pull the system away from the oscillatory regime.

6. Conclusions

The AMOC streamfunction calculated in density space was compared to the AMOC in the more commonly used

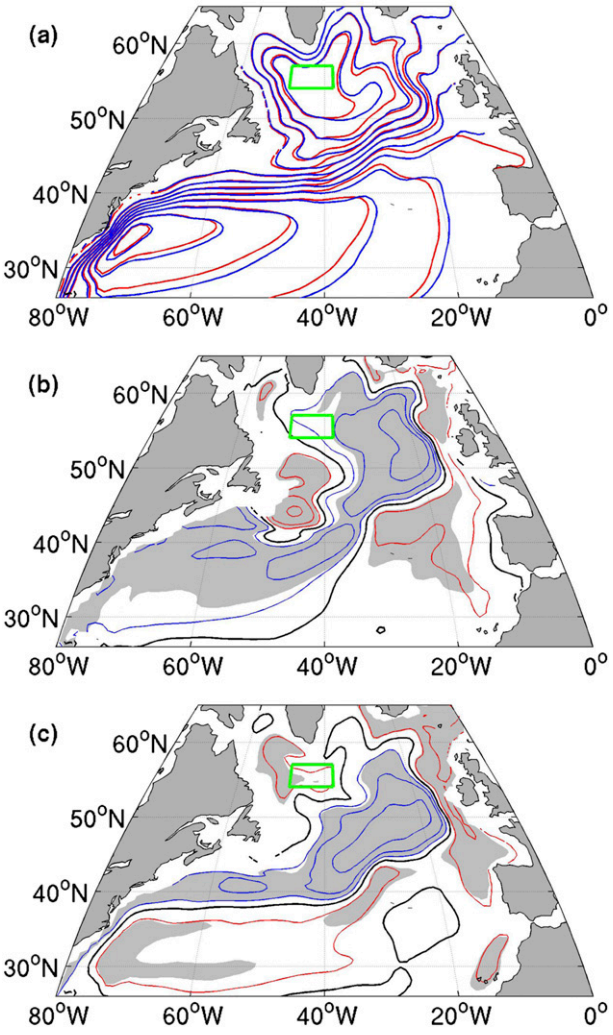

FIG. 14. (a) Mean upper 500-m depth-integrated streamfunction in regime 1 (red) and regime 2 (blue). Contour interval is 5 Sv. Also shown are lag correlations between the upper 500-m density and the convection index when the density lags the convection index time series by 7 years in (b) regime 1 and (c) regime 2. Positive (negative) correlations are plotted in red (blue). Contour interval is 0.2. Shading indicates significance at the 5% level. The green boxes denote the location of the convection site.

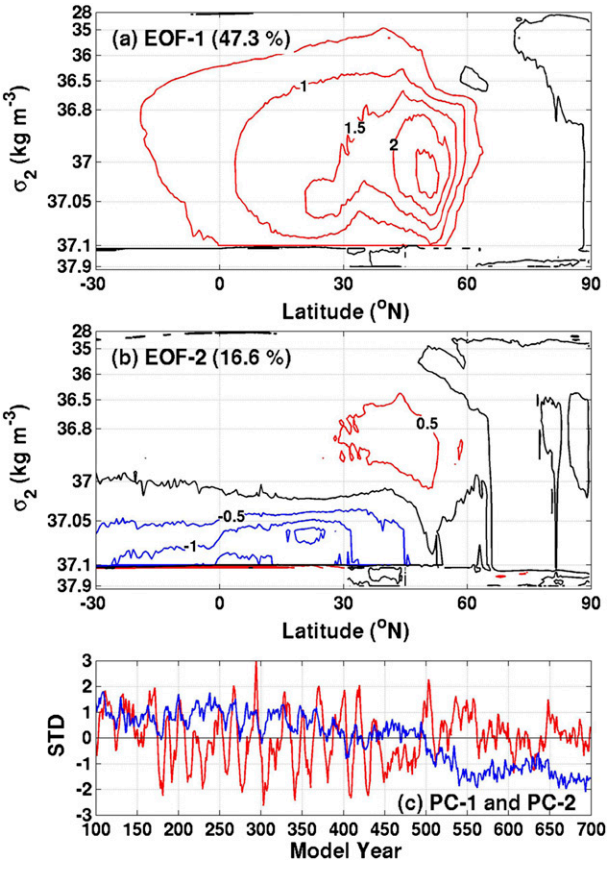

FIG. 15. (a),(b) Leading EOF patterns of the density coordinate AMOC for years 100–699. Amplitudes correspond to a one standard deviation change of the corresponding PC. Contour interval is 0.5 Sv. Positive (negative) anomalies are plotted in red (blue). Portion of the total variance explained by each mode is noted in the parentheses. Also show are the (c) PC1 (red) and PC2 (blue) time series.

depth space to diagnose the mechanism of multidecadal AMOC variability in the 700-yr present-day control integration of CCSM3. The largest difference between the two representations occurs in the subpolar gyre where the isopycnal surfaces deviate greatly from the depth levels due to the continuous buoyancy loss along the cyclonic gyre circulation and the doming near the center of the gyre. The density-based AMOC primarily reflects upper ocean changes along the subpolar gyre circulation, hence the AMOC anomalies in density space propagate northward in the subpolar region. On the other hand, the depth-based AMOC dominantly shows the changes in the deep equatorward circulation following the deep water formation in the western subpolar gyre, so the AMOC anomalies propagate equatorward in depth space.

As the two AMOC representations highlight the contributions from the distinct components of the circulation (with the correlation between the two maximum AMOC time series being merely 0.52), the combined information from the two led us to a more complete understanding of the ~20-yr AMOC variability in CCSM3 regime 1. The coupling of the deep and upper ocean circulation associated with deep convection changes at the main convection site and the crossover between the North Atlantic Current and the deep equatorward flow near the western flank of the Mid-Atlantic Ridge were shown to be the key elements of the ~20-yr oscillation. In response to a weakening of the equatorward deep transport (i.e., in the weak AMOC phase), the North

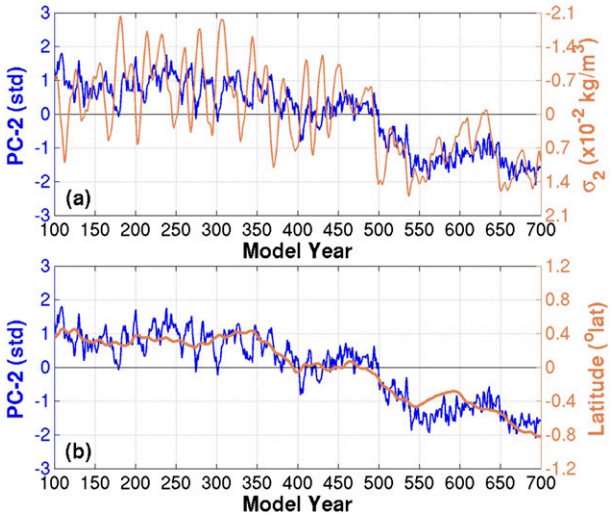

FIG. 16. (a) PC2 time series of the density coordinate AMOC for years 100–699 (blue) and the 2000–3000-m density anomalies (σ_2) averaged in the subpolar gyre (40°–65°N, 30°–60°W) (brown). Note that the right-hand *y* axis for the density is reversed. (b) PC2 (blue) and the anomalies of the North Atlantic Current at 30°W smoothed with 200-yr moving average (brown).

Atlantic Current shifts south and creates positive density anomalies in upper ocean, (and conversely from the deep transport strengthening). These positive density anomalies are advected northward and progressively expand in the cyclonic subpolar gyre, so that in about 5 yr, the whole upper subpolar gyre becomes denser. The resulting enhanced deep water formation then leads to a strengthening of the equatorward return flow in the deep ocean and the AMOC. The stronger deep flow and AMOC originating in the subpolar region expand equatorward and reach the subpolar–subtropical gyre boundary in another approximately 5 yr, driving the North Atlantic Current path northward, which concludes the half of the ~20-yr cycle. Therefore, the half cycle of the ~20-yr AMOC oscillation from the southward to the northward shifts of the North Atlantic Current path (or equivalently from the maximum to the minimum deep convection) consists of about 5 yr of northward anomaly propagation in upper ocean (the upper AMOC branch) leading up to the convection changes and about 5 yr of equatorward anomaly propagation in the deep ocean (the deep AMOC branch) following the convection changes, with the interaction between the two branches and bottom topography playing a key role.

The meridional shift of the North Atlantic Current path in response to the changes in the strength of the AMOC and deep return flow was shown to be consistent with previous theoretical, observational, and modeling studies that suggested a southward shift of the Gulf Stream in response to a stronger Deep Western Boundary Current (Thompson and Schmitz 1989; Spall 1996a,b; Zhang and Vallis 2007; Peña-Molino and Joyce 2008), despite the seemingly opposite direction of the path shift. Indeed, the crossover between the deep and upper ocean currents in CCSM3 is near the western flank of the Mid-Atlantic Ridge, while it is near the western boundary in the above studies. Therefore, the much more gentle and opposite zonal slope of the topography results in the opposite bottom torque and thus the opposite shift of the North Atlantic Current path. In fact, in regime 1 the Gulf Stream path near the western boundary shifts in the opposite direction to that of the North Atlantic Current path farther downstream in response to the AMOC change, as shown by Figs. 9b,c and 14b (see also Frankignoul et al. 2013). This opposite shift first appears near the tail of the Grand Banks and then farther south, as the anomalous deep return flow first increases near the tail of the Grand Banks almost simultaneously with the western flank of the Mid-Atlantic Ridge, while it intensifies later near Cape Hatteras (Fig. 6).

As most ocean general circulation models do not have sufficient horizontal resolution to realistically simulate the northern recirculation gyre and the Deep Western Boundary Current, our explanation for the CCSM3 may also apply to the previous studies based on coarse-resolution ocean models (e.g., de Coëtlogon et al. 2006; Kwon et al. 2010). In any case, the differences in the meridional shifts of the North Atlantic Current and Gulf Stream paths should be examined in the observations, especially in light of the recent observational evidences of the interior pathways of the deep return flow (Bower et al. 2009).

The changes in the propagation speed of the deep ocean circulation anomalies were noteworthy. The AMOC anomalies following deep convection changes expanded equatorward rapidly in the subpolar region (50°–60°N) along the western boundary topographic waveguide. This was followed by a much slower advection along the interior pathway from the Flemish Cap to the western flank of the Mid-Atlantic Ridge and then westward to Cape Hatteras, before finally speeding up again along the western boundary topographic waveguide to the south of Cape Hatteras. This is consistent with findings by Zhang (2010b) for the Geophysical Fluid Dynamics Laboratory Coupled Model, version 2.1 (GFDL CM2.1). However, it remains to be established whether the existence of these interior pathway for the deep return flow is physically consistent with the observations and eddy-resolving model simulations (Bower et al. 2009; Gary et al. 2011) or is primarily due to the insufficient horizontal resolution of these climate models.

The transition from the strong ~20-yr periodicity to more irregular and weaker red noise–like AMOC variability in CCSM3 is found to be due the slow model drift in the deep ocean toward a denser and colder state. The increased vertical stability in the main convection site due to the denser deep ocean limits the depth of deep convection, resulting in a change in AMOC behavior. Danabasoglu et al. (2010) and Yeager and Danabasoglu (2012) examined the impact of the denser deep subpolar gyre more systematically by comparing the CCSM4 with and without the new Nordic seas overflow parameterization. Even though the denser deep subpolar gyre resulted from a completely different cause, the consequence on the deep convection and AMOC maximum strength are consistent with our CCSM3 results.

Born et al. (2013) and Born and Stocker (2014) suggested that the subpolar gyre is bistable due to a positive feedback between the deep convection and salt advection by subpolar gyre: one mode with stronger subpolar gyre and active convection, and the other with weaker subpolar gyre and convection, which is consistent with the changes in subpolar gyre and convection between the regime 1 and regime 2 in CCSM3. However, the upper ocean salinity becomes slightly saltier at the convection site in regime 2, which does not support the key role of salinity convergence due to the subpolar gyre.

As summarized in the introduction, the NAO is closely related to the deep water formation and subpolar gyre circulation in both regimes (Danabasoglu 2008; Kwon and Frankignoul 2012). A positive NAO drives increased deep water formation due to increased heat loss from ocean and thermocline doming in the subpolar gyre, resulting in an AMOC intensification. Hence, the NAO acts as stochastic forcing for the AMOC variability, but does not directly determine its time scale, as schematically indicated in Fig. 13. Perhaps the stochastic NAO forcing acting on the slow background changes makes the transition from the regime 1 to regime 2 relatively abrupt and nonlinear.

The prominent role of NAO as the driving force of the observed changes of the subpolar gyre in the last few decades has been emphasized in many studies. For example, the remarkable rapid warming of the subpolar gyre SST in mid-1990 has been attributed to the strengthening of AMOC in response to the prolonged positive NAO (Robson et al. 2012; Yeager et al. 2012). Also, the subpolar gyre cooling in 1960s and again in recent decade are attributed to a weaker AMOC and associated decrease in the subpolar gyre heat flux convergence (Robson et al. 2014; Hermanson et al. 2014). While these relationships among the NAO, AMOC, and subpolar gyre circulation are consistent with those in CCSM3, the observed decadal changes are mostly related to the decadal changes in NAO, which are larger than in the present control simulation. In addition, the observational record is too short for a detailed comparison.

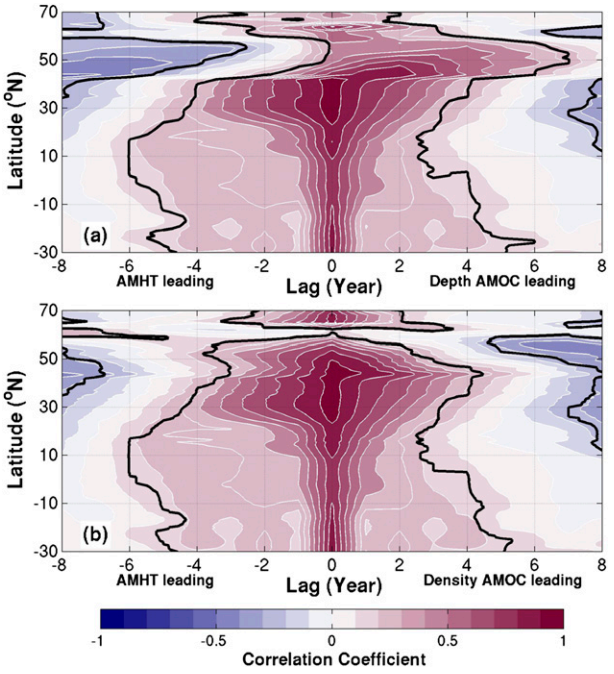

FIG. 17. Lag correlation between the maximum AMOC time series at each latitude and the Atlantic meridional heat transport (AMHT) at the same latitude in regime 1 for (a) depth coordinate AMOC and (b) density coordinate AMOC. Positive (negative) lags indicate the AMOC leads (lags) the AMHT at the same latitude. Contour interval is 0.1. Black contours indicate the significance at the 5% level.

In this study, we showed the utility of considering the AMOC in density space when analyzing its multidecadal variability. In addition, the AMOC in density space is more closely related to the meridional ocean heat transport, especially in the subpolar gyre (Fig. 17), as the meridional ocean heat transport is dominated by the upper ocean circulation (Boccaletti et al. 2005; Ferrari and Ferreira 2011). The AMOC in density space is highly correlated in phase with the meridional ocean heat transport at all latitudes, while in the subpolar gyre the depth AMOC exhibits a significant time lag with the meridional heat transport at the same latitude (Fig. 17). However, while the AMOC in density space clearly reflects the role of the upper ocean subpolar gyre in CCSM3, the results could differ in other models depending on the relative strength of the subpolar gyre. For example, Zhang (2010b) showed that the density AMOC from GFDL CM2.1 primarily reflects the equatorward AMOC propagation even in the subpolar region. Nonetheless, our approach based on the comparison of

two representations of the AMOC may be useful, and the proposed mechanism for the strong oscillatory AMOC multidecadal variability in CCSM3 may apply to other climate models, as many climate models indeed exhibit strong AMOC oscillations (often with ~20-yr time scale), which are an important source of decadal predictability (e.g., Msadek et al. 2010).

Acknowledgments. Support from the NOAA Climate Program Office (Grant NA10OAR4310202 and NA13OAR4310139) and NSF EaSM2 (OCE1242989) is gratefully acknowledged. We thank Gokhan Danabasoglu, Guillaume Gastineau, Mike Spall, Jiayan Yang, and Steve Yeager for helpful discussions, and the three anonymous reviewers and the editor Peter Gent for their thoughtful comments.

REFERENCES

Boccaletti, G., R. Ferrari, A. Adcroft, D. Ferreira, and J. Marshall, 2005: The vertical structure of ocean heat transport. *Geophys. Res. Lett.,* **32,** L10603, doi:10.1029/2005GL022474.

Born, A., and T. F. Stocker, 2014: Two stable equilibria of the Atlantic subpolar gyre. *J. Phys. Oceanogr.,* **44,** 246–264, doi:10.1175/JPO-D-13-073.1.

——, ——, C. C. Raible, and A. Levermann, 2013: Is the Atlantic subpolar gyre bistable in comprehensive coupled climate models? *Climate Dyn.,* **40,** 2993–3007, doi:10.1007/s00382-012-1525-7.

Bower, A. S., M. S. Lozier, S. F. Gary, and C. W. Böning, 2009: Interior pathways of the North Atlantic meridional overturning circulation. *Nature,* **459,** 243–248, doi:10.1038/nature07979.

Bretherton, C. S., M. Widman, V. P. Dymnikov, J. M. Wallace, and I. Bladé, 1999: The effective number of spatial degrees of freedom of a time-varying field. *J. Climate,* **12,** 1990–2009, doi:10.1175/1520-0442(1999)012<1990:TENOSD>2.0.CO;2.

Bryan, F. O., F. Danabasoglu, N. Nakashiki, Y. Yoshida, D.-H. Kim, J. Tsutsui, and S. C. Doney, 2006: Response of the North Atlantic thermohaline circulation and ventilation to increasing carbon dioxide in CCSM3. *J. Climate,* **19,** 2382–2397, doi:10.1175/JCLI3757.1.

Collins, W. D., and Coauthors, 2006: The Community Climate System Model version 3 (CCSM3). *J. Climate,* **19,** 2122–2143, doi:10.1175/JCLI3761.1.

Danabasoglu, G., 2008: On multidecadal variability of the Atlantic meridional overturning circulation in the Community Climate System Model version 3 (CCSM3). *J. Climate,* **21,** 5524–5544, doi:10.1175/2008JCLI2019.1.

——, W. G. Large, and B. P. Briegleb, 2010: Climate impacts of parameterized Nordic Sea overflows. *J. Geophys. Res.,* **115,** C11005, doi:10.1029/2010JC006243.

——, S. G. Yeager, Y.-O. Kwon, J. J. Tribbia, A. S. Phillips, and J. Hurrell, 2012: Variability of the Atlantic meridional overturning circulation in CCSM4. *J. Climate,* **25,** 5153–5172, doi:10.1175/JCLI-D-11-00463.1.

de Coëtlogon, G., C. Frankignoul, M. Bentsen, C. Delon, H. Haak, S. Massina, and A. Pardaens, 2006: Gulf Stream variability in five oceanic general circulation models. *J. Phys. Oceanogr.,* **36,** 2119–2135, doi:10.1175/JPO2963.1.

Delworth, T. L., and R. J. Greatbatch, 2000: Multidecadal thermohaline circulation variability driven by atmospheric surface flux forcing. *J. Climate,* **13,** 1481–1495, doi:10.1175/1520-0442(2000)013<1481:MTCVDB>2.0.CO;2.

Deshayes, J., and C. Frankignoul, 2008: Simulated variability of the circulation in the North Atlantic from 1953 to 2003. *J. Climate,* **21,** 4919–4933, doi:10.1175/2008JCLI1882.1.

Döös, K., and D. J. Webb, 1994: The Deacon cell and the other meridional cells of the Southern Ocean. *J. Phys. Oceanogr.,* **24,** 429–442, doi:10.1175/1520-0485(1994)024<0429:TDCATO>2.0.CO;2.

Ferrari, R., and D. Ferreira, 2011: What processes drive the ocean heat transport? *Ocean Modell.,* **38,** 171–186, doi:10.1016/j.ocemod.2011.02.013.

Frankignoul, C., G. Gastineau, and Y.-O. Kwon, 2013: The influence of the AMOC variability on the atmosphere in CCSM3. *J. Climate,* **26,** 9774–9790, doi:10.1175/JCLI-D-12-00862.1.

Gary, S. F., M. S. Lozier, C. W. Böning, and A. Biastoch, 2011: Deciphering the pathways for the deep limb of the meridional overturning circulation. *Deep-Sea Res. II,* **58,** 1781–1797, doi:10.1016/j.dsr2.2010.10.059.

Hawkins, E., and R. Sutton, 2007: Variability of the Atlantic thermohaline circulation described by three-dimensional empirical orthogonal functions. *Climate Dyn.,* **29,** 745–762, doi:10.1007/s00382-007-0263-8.

Hermanson, L., R. Eade, N. H. Robinson, N. J. Dunstone, M. B. Andrews, J. R. Knight, A. A. Scaife, and D. M. Smith, 2014: Forecast cooling of the Atlantic subpolar gyre and associated impacts. *Geophys. Res. Lett.,* **41,** 5167–5174, doi:10.1002/2014GL060420.

Hogg, N. G., and H. M. Stommel, 1985: On the relation between the deep circulation and the Gulf Stream. *Deep-Sea Res.,* **32,** 1181–1193, doi:10.1016/0198-0149(85)90002-0.

Knight, J. R., R. J. Allan, C. K. Folland, M. Vellinga, and M. E. Mann, 2005: A signature of persistent natural thermohaline circulation cycles in observed climate. *Geophys. Res. Lett.,* **32,** L20708, doi:10.1029/2005GL024233.

Kwon, Y.-O., and C. Frankignoul, 2012: Stochastically-driven multidecadal variability of the Atlantic meridional overturning circulation in CCSM3. *Climate Dyn.,* **38,** 859–876, doi:10.1007/s00382-011-1040-2.

——, M. A. Alexander, N. A. Bond, C. Frankignoul, H. Nakamura, B. Qiu, and L. Thompson, 2010: Role of Gulf Stream and Kuroshio–Oyashio systems in large-scale atmosphere–ocean interaction: A review. *J. Climate,* **23,** 3249–3281, doi:10.1175/2010JCLI3343.1.

Mauritzen, C., and S. Häkkinen, 1999: On the relationship between dense water formation and the ''meridional overturning cell'' in the North Atlantic Ocean. *Deep-Sea Res.,* **46,** 877–894, doi:10.1016/S0967-0637(98)00094-6.

Msadek, R., K. W. Dixon, T. Delworth, and W. Hurling, 2010: Assessing the predictability of the Atlantic meridional overturning circulation and associated fingerprints. *Geophys. Res. Lett.,* **37,** L19608, doi:10.1029/2010GL044517.

——, W. E. Johns, S. G. Yeager, G. Danabasoglu, T. L. Delworth, and A. Rosati, 2013: The Atlantic meridional heat transport at 26.5°N and its relationship with the MOC in the RAPID array and the GFDL and NCAR coupled models. *J. Climate,* **26,** 4335–4356, doi:10.1175/JCLI-D-12-00081.1.

Peña-Molino, B., and T. M. Joyce, 2008: Variability in the slope water and its relation to the Gulf Stream path. *Geophys. Res. Lett.,* **35,** L03606, doi:10.1029/2007GL032183.

Pickart, R. S., and M. A. Spall, 2007: Impact of Labrador Sea convection on the North Atlantic meridional overturning circulation. *J. Phys. Oceanogr.,* **37,** 2207–2227, doi:10.1175/JPO3178.1.

Robson, J., R. Sutton, K. Lohmann, D. Smith, and M. D. Palmer, 2012: Causes of the rapid warming of the North Atlantic Ocean in the mid-1990s. *J. Climate,* **25,** 4116–4134, doi:10.1175/JCLI-D-11-00443.1.

——, ——, and D. Smith, 2014: Decadal predictions of the cooling and freshening of the North Atlantic in the 1960s and the role of ocean circulation. *Climate Dyn.,* **42,** 2353–2365, doi:10.1007/s00382-014-2115-7.

Spall, M. A., 1996a: Dynamics of the Gulf Stream/deep western boundary current crossover. Part I: Entrainment and recirculation. *J. Phys. Oceanogr.,* **26,** 2152–2168, doi:10.1175/1520-0485(1996)026<2152:DOTGSW>2.0.CO;2.

——, 1996b: Dynamics of the Gulf Stream/deep western boundary current crossover. Part II: Low-frequency internal oscillations. *J. Phys. Oceanogr.,* **26,** 2169–2182, doi:10.1175/1520-0485(1996)026<2169:DOTGSW>2.0.CO;2.

Straneo, F., 2006: On the connection between dense water formation, overturning, and poleward heat transport in a convective basin. *J. Phys. Oceanogr.,* **36,** 1822–1840, doi:10.1175/JPO2932.1.

Thompson, J. D., and W. J. Schmitz, 1989: A limited area model of the Gulf Stream: Design, initial experiments, and model–data intercomparison. *J. Phys. Oceanogr.,* **19,** 791–814, doi:10.1175/1520-0485(1989)019<0791:ALAMOT>2.0.CO;2.

Trenberth, K. E., 1984: Some effects of finite sample size and persistence on meteorological statistics. Part I: Autocorrelations. *Mon. Wea. Rev.,* **112,** 2359–2368, doi:10.1175/1520-0493(1984)112<2359:SEOFSS>2.0.CO;2.

Tulloch, R., and J. Marshall, 2012: Exploring mechanisms of variability and predictability of Atlantic meridional overturning circulation in two coupled climate models. *J. Climate,* **25,** 4067–4080, doi:10.1175/JCLI-D-11-00460.1.

Yeager, S., and G. Danabasoglu, 2012: Sensitivity of Atlantic meridional overturning circulation variability to parameterized Nordic Sea overflows in CCSM4. *J. Climate,* **25,** 2077–2103, doi:10.1175/JCLI-D-11-00149.1.

——, A. Karspeck, G. Danabasoglu, J. Tribbia, and H. Teng, 2012: A decadal prediction case study: Late twentieth-century North Atlantic Ocean heat content. *J. Climate,* **25,** 5173–5189, doi:10.1175/JCLI-D-11-00595.1.

Zhang, R., 2010a: Northward intensification of anthropogenically forced changes in the Atlantic meridional overturning circulation (AMOC). *Geophys. Res. Lett.,* **37,** L24603, doi:10.1029/2010GL045054.

——, 2010b: Latitudinal dependence of Atlantic meridional overturning circulation (AMOC) variations. *Geophys. Res. Lett.,* **37,** L16703, doi:10.1029/2010GL044474.

——, and G. K. Vallis, 2007: The role of bottom vortex stretching on the path of the North Atlantic western boundary current and on the northern recirculation gyre. *J. Phys. Oceanogr.,* **37,** 2053–2080, doi:10.1175/JPO3102.1.

Zhu, X., and J. Jungclaus, 2008: Interdecadal variability of the meridional overturning circulation as an ocean internal mode. *Climate Dyn.,* **31,** 731–741, doi:10.1007/s00382-008-0383-9.